CrossMark

LISA Galactic Binaries with Astrometry from Gaia DR3

Thomas Kupfer[1,2,18] , Valeriya Korol[3,4,18] , Tyson B. Littenberg[5] , Sweta Shah[6,7] , Etienne Savalle[8,9] ,
Paul J. Groot[10,11,12] , Thomas R. Marsh[13] , Maude Le Jeune[8], Gijs Nelemans[10,14,15] , Anna F. Pala[16] , Antoine Petiteau[8,9] ,
Gavin Ramsay[17] , Danny Steeghs[13] , and Stanislav Babak[8]

[1] Hamburger Sternwarte, University of Hamburg, Gojenbergsweg 112, 21029 Hamburg, Germany
[2] Department of Physics and Astronomy, Texas Tech University, P.O. Box 41051, Lubbock, TX 79409, USA
[3] Max-Planck-Institut für Astrophysik, Karl-Schwarzschild-Straße 1, 85741 Garching, Germany
[4] Institute for Gravitational Wave Astronomy, School of Physics and Astronomy, University of Birmingham, Birmingham, B15 2TT, UK
[5] NASA Marshall Space Flight Center, Huntsville, AL 35811, USA
[6] Max Planck Institute for Gravitational Physics (Albert Einstein Institute), Callinstrasse 38, 30167 Hannover, Germany
[7] Leibniz Universität Hannover, Institut für Gravitationsphysik, Callinstrasse 38, 30167 Hannover, Germany
[8] Université de Paris, CNRS, Astroparticule et Cosmologie, 75013 Paris, France
[9] IRFU, CEA, Université Paris-Saclay, F-91191, Gif-sur-Yvette, France
[10] Department of Astrophysics/IMAPP, Radboud University, P.O. Box 9010, 6500 GL Nijmegen, The Netherlands
[11] South African Astronomical Observatory, P.O. Box 9, Observatory, 7935, Cape Town, South Africa
[12] Department of Astronomy & Inter-University Institute for Data Intensive Astronomy, University of Cape Town, Private Bag X3, 7701 Rondebosch, South Africa
[13] Department of Physics, University of Warwick, Gibbet Hill Road, Coventry CV4 7AL, UK
[14] SRON, Netherlands Institute for Space Research, Niels Bohrweg 4, 2333 CA Leiden, The Netherlands
[15] Institute of Astronomy, KU Leuven, Celestijnenlaan 200D, B-3001 Leuven, Belgium
[16] European Space Agency, European Space Astronomy Centre, Camino Bajo del Castillo s/n, 28692 Villanueva de la Cañada, Madrid, Spain
[17] Armagh Observatory and Planetarium, College Hill, Armagh BT61 9DG, UK

Abstract

Galactic compact binaries with orbital periods shorter than a few hours emit detectable gravitational waves (GWs) at low frequencies. Their GW signals can be detected with the future Laser Interferometer Space Antenna (LISA). Crucially, they may be useful in the early months of the mission operation in helping to validate LISA's performance in comparison to prelaunch expectations. We present an updated list of 55 candidate LISA-detectable binaries with measured properties, for which we derive distances based on Gaia Data Release 3 astrometry. Based on the known properties from electromagnetic observations, we predict the LISA detectability after 1, 3, 6, and 48 months using Bayesian analysis methods. We distinguish between verification and detectable binaries as being detectable after 3 and 48 months, respectively. We find 18 verification binaries and 22 detectable sources, which triples the number of known LISA binaries over the last few years. These include detached double white dwarfs, AM CVn binaries, one ultracompact X-ray binary, and two hot subdwarf binaries. We find that across this sample the GW amplitude is expected to be measured to $\approx 10\%$ on average, while the inclination is expected to be determined with $\approx 15°$ precision. For detectable binaries, these average errors increase to $\approx 50\%$ and $\approx 40°$, respectively.

1. Introduction

Binary systems composed of degenerate stellar remnants (white dwarfs, neutron stars, and black holes) in orbits with periods of less than a few hours are predicted to be strong gravitational-wave (GW) sources in our own Galaxy. A number of these systems—primarily consisting of a neutron star or white dwarf paired with a compact helium star, white dwarf, or another neutron star—have been identified primarily through the observation in optical and X-ray electromagnetic (EM) wave bands. Some of these systems display remarkably short orbital periods, down to just several minutes (e.g., Amaro-Seoane et al. 2023). Binaries in such a tight orbit emit GWs at megahertz frequencies that can be detected directly with the future Laser Interferometer Space Antenna (LISA;

Amaro-Seoane et al. 2017), and other future planned space-based GW observatories such as TianQin (Luo et al. 2016; Huang et al. 2020), Taiji (Ruan et al. 2018), and the Lunar Gravitational Wave Antenna (Harms et al. 2021).

In this study, we focus on the LISA mission, which is a European Space Agency (ESA)-led GW observatory currently scheduled for launch in the mid-2030s.[19] Designed to operate in the frequency band between 0.1 and 100 mHz (Amaro-Seoane et al. 2017), LISA is an ideal tool for discovering massive black hole mergers and extreme/intermediate-mass ratio inspirals. In addition, it can survey the shortest period stellar remnant binaries throughout the entire Milky Way, providing a complementary view of our Galaxy for EM surveys (for a review see Amaro-Seoane et al. 2023). Both theory- and observation-based studies find that LISA will deliver a sample of $\mathcal{O}(10^4)$ binaries with orbital periods of <1 hr, which will be complete up to periods of <15 minutes (e.g., Nelemans et al. 2001; Ruiter et al. 2009; Nissanke et al. 2012; Lamberts et al. 2019; Breivik et al. 2020; Li et al. 2020;

---

[18] Both authors contributed equally to this work.

[19] https://sci.esa.int/web/lisa/-/61367-mission-summary

Korol et al. 2022). A significant number of $\mathcal{O}(10^2)$ of stellar remnant binaries—primarily those composed of two white dwarfs—discovered by LISA will be possible to study in combination with EM surveys (e.g., Nelemans et al. 2004; Marsh 2011; Korol et al. 2017; Breivik et al. 2018; Tauris 2018; Li et al. 2020).

In the context of the LISA mission, stellar remnant binaries known from EM observations are often termed *verification binaries*, based on the idea that one can model their GW signal using EM measurements of the binary's parameters and can employ these to test LISA data quality (e.g., Ströer & Vecchio 2006; Littenberg 2018; Savalle et al. 2022). In our previous work, we reviewed a sample of candidate LISA verification binaries following Gaia Data Release 2 (DR2). This allowed us to determine distances—previously highly uncertain for most binaries—based on Gaia's parallax measurements (Kupfer et al. 2018; Ramsay et al. 2018). In turn, new distance estimates enabled us to evaluate the uncertainty on the expected GW signal's amplitude and to assess the detectability of these candidate verification binaries with LISA. In this work, we update the sample of candidate LISA verification binaries in a number of ways. First, we include several newly discovered systems since Gaia DR2 (Section 2). Second, we reevaluate the distances based on improved astrometry from Gaia Data Release 3 (DR3), while also taking into account their proper motion information (Section 3.3). In addition, we evaluate their detectability as well as the binary parameter estimation in a fully Bayesian way using the up-to-date LISA sensitivity requirements (Section 3.4).

So far verification binaries have been (arbitrarily) defined as such based on an assumed signal-to-noise ratio (S/N) detection threshold reached at a set observation time. However, this definition relies on a few caveats. First, the S/N threshold and the integration time needed to make an unambiguous identification of a (known) source is not just a matter of the source's intrinsic amplitude, but is also heavily dependent on the realization of the rest of the Galactic population (i.e., unresolved Galactic confusion foreground) that the source is competing against (e.g., Figure 4 of Korol et al. 2023). In addition, the Galactic confusion foreground is dynamic: it will decrease with time as more and more sources will become detectable and will become individually resolved. Moreover, LISA's orbit around the Sun will introduce a modulation in the Galactic foreground reaching its maximum when LISA is optimally oriented toward the Galactic center, which is where the density of Galactic sources peaks (e.g., Petiteau 2008). A prototype global fit data analysis pipeline for LISA demonstrated that the Galactic foreground subtraction steadily improves with time with a few $\mathcal{O}(10^3)$ binaries being identified (and subtracted) already after 1 month (Littenberg & Cornish 2023). Moreover, known binaries will be the most crucial in the early weeks/months of the mission operation in helping to validate the early performance of the instrument in comparison to prelaunch expectations. It is therefore reasonable to expect that the first data validation may be required after only a few months from the beginning of science operations. We anticipate that an integration time as short as 1–3 months would allow for basic consistency tests on the recovered parameters on a few epochs of commissioning data for several verification binaries. Given all of the above, in this study, we opt to call as *verification binary* a system that becomes detectable, which is judged based on the shape of the recovered

posteriors on binary's parameters rather than an S/N threshold, within 3 months of observation time with LISA, and we call a as *detectable binary* when it is detected after 48 months (at present set as the nominal lifetime of the mission).

2. The Sample of Compact LISA Sources Since Gaia DR2

At present the catalog of candidate verification binaries includes detached (Brown et al. 2016a) and semidetached double white dwarfs (DWDs; the latter called AM CVn type binaries; see Solheim (2010) for a recent review), hot subdwarf stars with a white dwarf companion (see Geier et al. 2013; Pelisoli et al. 2021; Kupfer et al. 2022 for recent discoveries), semidetached white dwarf-neutron star binaries (so-called ultracompact X-ray binaries; Nelemans & Jonker 2010), double neutron stars (Lyne et al. 2004) and cataclysmic variables (CVs; Scaringi et al. 2023). In Kupfer et al. (2018), we analyzed ∼50 known candidates using distances derived from parallaxes provided in the Gaia DR2 catalog (Gaia Collaboration et al. 2018). We found that 13 candidates exceed an S/N threshold of 5 for a LISA mission duration of 4 yr.

The Zwicky Transient Facility (ZTF) performed a dedicated high-cadence survey to find short-period binaries (Kupfer et al. 2021). More than 20 new binary systems with orbital periods ranging from 7 minutes to ≈1 hr have been discovered by ZTF since the beginning of science operations in 2018 March (Bellm 2014; Burdge et al. 2019a, 2020b; Kupfer et al. 2020a, 2020b; Burdge et al. 2020b; van Roestel et al. 2022; Burdge et al. 2023). This new sample includes eight eclipsing systems, seven AM CVn systems, and six systems exhibiting primarily ellipsoidal variations in their light curves. Remarkably, one of the first ZTF discoveries was the shortest orbital period detached eclipsing binary system known to date, ZTF J1539+5027, with a period of just 6.91 minutes (Burdge et al. 2019a). Owing both to its inherently high GW frequency and large GW amplitude, ZTF J1539+5027 is expected to be one of the loudest Galactic GW sources and could reach the S/N detection threshold of ≈7 within a week. Littenberg & Cornish (2019) showed that for high-frequency systems like ZTF J1539 +5027, GW measurements will independently provide comparable levels of precision to the current EM measurement of the orbital evolution of the system, and will improve the precision to which the distance and orientation is known.

The Extremely Low Mass (ELM) white dwarf survey has successfully completed its observations across the footprint of the Sloan Digital Sky Survey (SDSS), and expanded its search to the Southern Hemisphere (Kosakowski et al. 2020; Brown et al. 2022; Kosakowski et al. 2023a). Over the last few years, the ELM survey discovered several sub-hour orbital period double degenerates, including the first double helium-core white dwarf binary (e.g., Brown et al. 2020; Kilic et al. 2021; Kosakowski et al. 2021, 2023b). It is expected that double helium-core white dwarfs and carbon/oxygen + helium-core white dwarfs dominate the population in the LISA band despite that they make up only 10% of the global DWD population (Lamberts et al. 2019).

Moreover, several additional candidates have been found in other large-scale surveys. SDSS J1337 was discovered as a double degenerate in early SDSS-V data with an orbital period of 99 minutes. The spectrum shows spectral lines from both components making it a double-lined system that provides precise system parameters (Chandra et al. 2021). Pelisoli et al. (2021) discovered a compact hot subdwarf binary with a

massive white dwarf companion in a 99 minute period orbit in the TESS sky survey. The total mass of the system is above the Chandrasekhar mass making the system a double degenerate supernova Ia progenitor. Scaringi et al. (2023) showed that three known CVs, namely, WZ Sge, VW Hyi, and EX Hya, could be individually resolved after 4 yr of LISA operation.

Since the release of Gaia DR2 a few years ago, numerous sky surveys have collectively tripled the number of identified candidate compact binaries. It is noteworthy, however, that these surveys employ a variety of detection techniques and analysis methods, leading to heterogeneity in the presentation of results. Table 1 offers an overview of the observational results for known sources detectable by LISA, as reported in the respective studies. The properties of all sources compiled for this publication are accessible to the public via the LISA Consortium's GitLab repository at https://gitlab.in2p3.fr/LISA/lisa-verification-binaries.

3. Methods

3.1. Improvements from Gaia DR2 to Gaia DR3

In 2018, Gaia DR2 released full astrometric solutions, including parallaxes, and proper motions for 1.3 billion sources (Gaia Collaboration et al. 2016, 2018). The release was based on observations taken between 2014 July and 2016 May. The parallaxes allowed us for the first time to calculate distances for a large sample of LISA detectable compact binaries. The distances in combination with the chirp mass provided the opportunity to calculate GW amplitudes and estimate the detectability for LISA (Kupfer et al. 2018). Until Gaia DR2 only a small sample of AM CVn binaries had parallax measurements using the Hubble Space Telescope (Roelofs et al. 2007).

About 2 yr after the second data release, the Gaia Early Data Release (eDR3) provided full astrometric solutions for 1.4 billion sources based on 34 months of observations (Gaia Collaboration et al. 2021). The released data included one additional year of Gaia data leading to a higher precision in the parallaxes and proper motions compared to DR2 as well as first time parallax measurements for several LISA sources, including ZTF J1905, ZTF J0127, SDSS J0935, V803 Cen and CR Boo. Generally, we find that the parallaxes improved by about 20%–30% between DR2 and eDR3, in particular for faint sources (Figure 1). Our list also contains six binaries with either a negative parallax or a parallax error close to 100%. These are ZTF J1539, ZTF J2243, V407 Vul, ZTF J1905, 4U 1830-30, and ZTF J2029. We anticipate that for these objects the distance estimate is dominated by the derived scale length prior (see Section 3.3). We note that distances can also be estimated through indirect methods. In particular, spectroscopic distances have been used for DWDs. For this work, we only include parallaxes to derive distances to be independent of spectroscopic models.

In June 2022, Gaia DR3 was released. Gaia DR3 included the same data as eDR3 and as such astrometric solutions did not improve between eDR3 and DR3. However, DR3 included a large amount of additional information, including orbital astrometric solutions for wide binaries with a clean solution (Gaia Collaboration et al. 2023). For the remainder of the paper, we will always refer to DR3 knowing that parallaxes and proper motions are the same for eDR3 and DR3.

3.2. Systems with Uncertain Parallax or Alternative Distance Estimates

Here, we take the opportunity to discuss a few systems with uncertain parallax or alternative distance estimates: HM Cnc, 4U 1830-30, V407 Vul, and ZTF J1905.

HM Cnc is the only remaining system with no parallax measurement. Therefore, the distance estimate of HM Cnc remains debated. Roelofs et al. (2010) estimated a distance of 5 kpc based on its properties, whereas Reinsch et al. (2007) estimated a distance of ≈ 2 kpc based on the observed flux. Most recently Munday et al. (2023) presented the discovery of $\ddot{f} = (-5.38 \pm 2.10) \times 10^{-27}$ Hz s^{-2} in HM Cnc. They concluded that HM Cnc is close to the period minimum and theoretical Modules for Experiments in Stellar Astrophysics (MESA)[20] calculations find a mass of $\approx 1\,M_\odot$ for the accretor and $\approx 0.17\,M_\odot$ for the donor. This result is in strong contradiction to the results presented in Roelofs et al. (2010) based on a spectroscopic analysis. Munday et al. (2023) also discussed different ways to measure the distance to HM Cnc and found values between 2 and 11 kpc. This shows the very large uncertainties of the system properties from EM studies. As a consequence, the expected GW amplitude also remains uncertain.

In practice, 4U 1830-30 also lacks a parallax measurement. However, it is located in the globular cluster NGC 6624, which allows for an independent distance estimate using color–magnitude diagrams with theoretical isochrones, or by using variable stars that follow known relations between their periods and absolute luminosities like RR Lyrae stars. NGC 6624 has a well-measured distance of 7972 ± 277 pc (Baumgardt & Vasiliev 2021), which we take as the distance for 4U 1830-30.

V407 Vul's optical counterpart is dominated by a component that matches a G-type star with a blue variable (Steeghs et al. 2006). It is still unknown whether this is a chance alignment or whether V407 Vul is a triple system where an ultracompact inner binary is orbited by a G-star companion. Companions in orbits with a multi-year orbital period can present themselves in Gaia DR3 data, either they are listed in the non-single star tables of Gaia DR3 (nss_two_body_orbit) or they have a nonzero value in the astrometric_excess_noise keyword in the gaia_source table. The latter is nonzero if the astrometric solution shows additional perturbations to a single-source solution, which could be an indication of an astrometric wobble if the G-star in V407 Vul is in a wide orbit (e.g., Belokurov et al. 2020; Penoyre et al. 2020). V407 Vul is not listed in the non-single star tables of Gaia DR3 (nss_two_body_orbit) and has an astrometric_excess_noise = 0 and astrometric_excess_noise_sig = 0 and therefore there is no indication in the current Gaia DR3 data set that the G-star is a wide companion to the inner ultracompact binary. However, we note that Gaia DR3 is only sensitive to few-year periods Longer periods would not yet show up as astrometric wobble and therefore we cannot exclude that the G-star has a period of more than a few years.

ZTF J1905 presents a particular challenge with its uncertain Gaia DR3 parallax ($\varpi = 1.8652 \pm 1.5428$). This parallax value would imply the system's absolute magnitude of ≈ 11 mag, which seems contradictory when compared to AM CVn binaries with similar orbital periods such as AM CVn or SDSS J1908. Typically, AM CVn systems in the orbital period

---

[20] MESA is an open-source 1D stellar evolution code: https://docs.mesastar.org/en/release-r23.05.1/.

Table 1
Physical Properties of the Known Verification and Detectable Binaries

Source	Ref.	Type	Orbital period (s)	l_{Gal} (deg)	b_{Gal} (deg)	BP − RP (mag)	M_G (mag)	m_1 ($M_\odot$)	m_2 ($M_\odot$)	ι (deg)
Verification Binaries										
HM Cnc	(1, 2)	AM CVn	321.529129(10)	206.9246	23.3952	0.246	6.54	0.55	0.27	$\approx$38
ZTF J1539	(3)	DWD*	414.7915404(29)	80.7746	50.5819	−0.263	8.44	$0.61^{+0.017}_{-0.022}$	0.21 ± 0.015	$84.15^{+0.64}_{-0.57}$
ZTF J2243	(4)	DWD*	527.934890(32)	104.1514	−5.4496	−0.160	9.33	$0.349^{+0.093}_{-0.074}$	$0.384^{+0.114}_{-0.074}$	$81.88^{+1.31}_{-0.69}$
V407 Vul	(5)	AM CVn*	569.396230(126)	57.7281	6.4006	1.535	7.76	[0.8 ± 0.11]	[0.177 ± 0.071]	[60]
ES Cet	(6)	AM CVn*	620.21125(30)	168.9684	−65.8632	−0.296	5.55	[0.8 ± 0.11]	[0.161 ± 0.064]	[60]
SDSS J0651	(7, 8)	DWD*	765.206543(55)	186.9277	12.6886	0.029	9.37	0.247 ± 0.015	0.49 ± 0.02	$86.9^{+1.6}_{-1.0}$
ZTFJ 0538	(9)	DWD*	866.60331(16)	186.8104	−6.2213	0.025	8.80	0.45 ± 0.05	0.32 ± 0.03	$85.43^{+0.07}_{-0.09}$
SDSS J1351	(10)	AM CVn	939.0(7.2)	328.5021	53.1240	−0.122	7.80	[0.8 ± 0.11]	[0.100 ± 0.040]	[60]
AM CVn	(11, 12)	AM CVn	1028.7322(3)	140.2343	78.9382	−0.283	6.66	0.68 ± 0.06	0.125 ± 0.012	43 ± 2
ZTF J1905	(9)	AM CVn*	1032.16441(62)	0.1945	1.0968	−0.066	11.47	[0.8 ± 0.11]	[0.090 ± 0.035]	70 ± 20
SDSS J1908	(13, 14)	AM CVn	1085.108(1)	70.6664	13.9349	−0.018	6.27	[0.8 ± 0.11]	[0.085 ± 0.034]	10 − 20
HP Lib	(15, 16)	AM CVn	1102.70(5)	352.0561	32.5467	−0.153	6.36	0.49 − 0.80	0.048-0.088	26-34
SDSS J0935	(17, 18)	DWD	1188(42)	176.0796	47.3776	0.455	9.82	0.312 ± 0.019	0.75 ± 0.24	[60]
J0526+5934	(19)	DWD	1230.374667(7)	151.9201	13.2614	0.186	7.92	$0.378^{+0.066}_{-0.060}$	$0.887^{+0.110}_{-0.098}$	$57.1^{+4.3}_{-4.1}$
J1239-2041	(20)	DWD	1350.432(11.232)	299.2755	42.0943	−0.072	9.00	0.291 ± 0.013	$0.68^{+0.11}_{-0.06}$	71^{+8}_{-10}
TIC 378898110	...	AM CVn	1347.96	297.0555	1.9451	0.027	6.82	[0.8 ± 0.11]	[0.10 ± 0.02]	74 ± 10
CR Boo	(16,21)	AM CVn	1471.3056(500)	340.9671	66.4884	0.066	7.74	0.67 − 1.10	0.044-0.088	30
SDSS0634	(22)	DWD	1591.4(28.9)	176.7322	13.3211	−0.189	8.95	$0.452^{+0.070}_{-0.062}$	$0.209^{+0.034}_{-0.021}$	37 ± 7
V803 Cen	(16, 23)	AM CVn	1596.4(1.2)	309.3671	20.7262	0.232	8.44	0.78 − 1.17	0.059-0.109	12-15
Detectable Binaries										
4U1820-30	(24, 25)	UCXB	685(4)	2.7896	−7.9144	...	3.7 (45)	[1.4]	[0.069]	[60]
ZTF J0127	(26)	DWD*	822.680314(43)	128.4671	−9.5102	.191	9.26	0.75 ± 0.06	0.19 ± 0.03	[75 − 90]
SDSS J2322	(27)	DWD	1201.4(5.9)	85.9507	−51.2104	−0.179	9.08	0.34 ± 0.02	>0.17	[60]
PTF J0533	(28)	DWD	1233.97298(17)	201.8012	−16.2238	−0.067	8.70	$0.652^{+0.037}_{-0.040}$	0.167 ± 0.030	$72.8^{+0.8}_{-1.4}$
ZTF J2029	(9)	DWD*	1252.0564909(41)	58.5836	−13.4655	−0.054	10.27	0.32 ± 0.04	0.30 ± 0.04	$86.64^{+0.70}_{-0.40}$
PTF 1J1919	(29)	AM CVn*	1347.354(20)	79.5945	15.5977	0.036	9.08	[0.8 ± 0.11]	[0.066 ± 0.026]	[60]
TIC 378898110	(30)	AM CVn	1347.96	297.0555	1.9451	0.027	6.82	[0.8 ± 0.11]	[0.1 ± 0.026]	74 ± 10
CXOGBS J1751	(31)	AM CVn	1374.0(6)	359.9849	−1.4108	1.623	6.01	[0.8 ± 0.11]	[0.064 ± 0.026]	[60]
ZTF J0722	(9)	DWD*	1422.548655(71)	232.9930	−1.8604	−0.157	8.23	0.38 ± 0.04	0.33 ± 0.03	89.66 ± 0.22
KL Dra	(32)	AM CVn	1501.806(30)	91.0140	19.1992	0.668	9.25	0.76	0.057	[60]
PTF 1J0719	(33)	AM CVn	1606.2(1.2)	168.6573	24.4945	0.425	9.30	[0.8 ± 0.11]	[0.053 ± 0.021]	[60]
CP Eri	(34, 35)	AM CVn	1740(84)	191.7021	−52.9098	0.218	10.5	[0.8 ± 0.11]	[0.049 ± 0.020]	[60]
SMSS J0338	(21)	DWD	1836.1(31.9)	128.8576	20.7792	−0.129	8.64	0.230 ± 0.015	$0.38^{+0.05}_{-0.03}$	69 ± 9
J2322+2103	(20)	DWD	1918.08(21.60)	96.5151	−37.1844	0.071	8.81	0.291 ± 0.013	0.75 ± 0.26	[60]
SDSS J0106	(36)	DWD	2345.76(1.73)	191.9169	31.9952	−0.223	10.30	0.188 ± 0.011	$0.57^{+0.22}_{-0.07}$	67 ± 13
SDSS J1630	(37)	DWD	2388.0(6.0)	67.0760	43.3604	−0.147	9.54	0.298 ± 0.019	0.76 ± 0.24	[60]
J1526m2711	(38)	DWD	2417.645(37.930)	340.4437	24.1935	−0.108	9.36	0.37 ± 0.02	>0.40 ± 0.02	[60]
SDSS J1235	(39, 40)	DWD	2970.432(4.320)	284.5186	78.0320	−0.219	9.27	0.35 ± 0.01	$0.27^{+0.06}_{-0.02}$	27.0 ± 3.8
SDSS J0923	(41)	DWD	3883.68(43.20)	195.8199	44.7754	−0.236	8.62	0.275 ± 0.015	0.76 ± 0.23	[60]
CD-30 11223	(42)	sdB*	4231.791855(155)	322.4875	28.9379	−0.388	4.55	0.54 ± 0.02	0.79 ± 0.01	82.9 ± 0.4
SDSS J1337	(43)	DWD	5942.952(300)	89.0428	74.0799	0.306	11.31	0.51 ± 0.01	0.32 ± 0.01	13 ± 1
HD 265435	(44)	sdB	5945.917432(280)	87.0170	1.1225	−0.425	3.76	$0.63^{+0.13}_{-0.12}$	1.01 ± 0.15	64^{+14}_{-5}

Notes. Masses and inclination angles in brackets are assumed and based on evolutionary stage and mass ratio estimations. Absolute magnitudes are calculated from the Gaia G-band magnitude in combination with our distance estimate.

References: (1) Strohmayer (2005), (2) Roelofs et al. (2010), (3) Burdge et al. (2019a), (4) Burdge et al. (2020b), (5) Ramsay & Hakala (2002), (6) Espaillat et al. (2005), (7) Brown et al. (2011), (8) Hermes et al. (2012), (9) Burdge et al. (2020b), (10) Green et al. (2018), (11) Skillman et al. (1999), (12) Roelofs et al. (2006), (13) Fontaine et al. (2011), (14) Kupfer et al. (2015), (15) Patterson et al. (2002), (16) Roelofs et al. (2007), (17) Brown et al. (2016b), (18) Kilic et al. (2014), (19) Kosakowski et al. (2023b), (20) Brown et al. (2022), (21) Provencal et al. (1997), (22) Kilic et al. (2021), (23) Anderson et al. (2005), (24) Stella et al. (1987), (25) Chen et al. (2020), (26) Burdge et al. (2023), (27) Brown et al. (2020), (28) Burdge et al. (2019a), (29) Levitan et al. (2014), (30) Green et al. (2024), (31) Wevers et al. (2016), (32) Wood et al. (2002), (33) Levitan et al. (2011), (34) Howell et al. (1991), (35) Groot et al. (2001), (36) Kilic et al. (2011b), (37) Kilic et al. (2011a), (38) Kosakowski et al. (2023a), (39) Kilic et al. (2017), (40) Breedt et al. (2017), (41) Brown et al. (2010), (42) Geier et al. (2013), (43) Chandra et al. (2021), (44) Pelisoli et al. (2021), (45) M_V taken from van Paradijs & McClintock (1994).
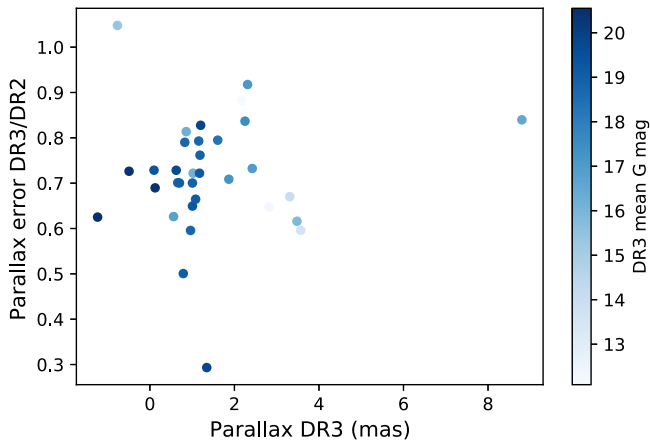
Figure 1. The error of the parallax in DR3 compared to DR2 for the verification sources in Tables 1 and 2. The color indicates the mean G mag of the source.

range between 15 and 20 minutes are much brighter, characterized by absolute magnitudes around 6.5 mag. There is no indication in the Gaia DR3 quality keywords that the parallax is problematic. Additionally, there is only modest extinction toward the direction of ZTF J1905. Green et al. (2019) report $E(g - r) = 0.18$, which results in an extinction of ≈ 0.5 mag in the Gaia G band, which is not sufficient to explain the apparent discrepancy. The distance of ZTF J1905 thus needs further investigation.

3.3. Distance Estimation

Gaia DR3 provides parallaxes that can be used to determine distances. To estimate distances from the measured parallaxes we use a probability-based inference approach (e.g., Bailer-Jones 2015; Astraatmadja & Bailer-Jones 2016; Igoshev et al. 2016; Bailer-Jones et al. 2018, 2021; Luri et al. 2018). We follow a similar approach as described in detail in Section 3.2 in Kupfer et al. (2018). The measured parallax follows a probability distribution and with a prior on the true distance distribution for the observed sources we can constrain the distance even if the parallax has large uncertainties. If the parallax uncertainty is below 10%–20% the distance estimate is independent of the prior. At larger uncertainties on the distance, the distance estimate becomes more and more dependent on the prior. We apply Bayes' theorem to measure the probability density for the distance

$$P(r|\varpi, \sigma_\varpi) = \frac{1}{Z}\, P(\varpi|d, \sigma_\varpi)\, P(d), \tag{1}$$

where d is the distance, $P(\varpi|r, \sigma_\varpi)$ is the likelihood function, which can be assumed to be Gaussian (Lindegren et al. 2018). $P(r)$ is the prior and Z is a normalization constant. As in Kupfer et al. (2018), we adopt an exponentially decreasing volume density prior $P(d)$

$$P(d) = \begin{cases} \dfrac{d^2}{2L^3}\exp(-d/L) & \text{if } d > 0 \\ 0 & \text{otherwise}, \end{cases} \tag{2}$$

where $L > 0$ is the scale length. Compared to our previous study, here we assume two values for L based on the binary's membership to the thin or thick disk as detailed below. We also

stress that for systems with poor parallax measurement, the distance estimate largely depends on our assumption for L.

To estimate if our candidate LISA binaries are members of the thin or thick disk, for each binary we calculate Galactic kinematics, i.e., velocity components and Galactic orbit. To do this, sky position, proper motions, systemic velocities, and distances are needed. We extract proper motions from Gaia DR3 and calculate the distance using Equations (1) and (2) by setting $L = 400$ or 795 pc; these are typical values for L for thin disk and thick disk objects, respectively.[21] Additionally, we use published systemic velocities, typically from radial velocity measurements. For systems with unknown systemic velocities, we assume $1 \pm 50\,\mathrm{km\,s^{-1}}$. As for the distance estimate, we calculate Galactic kinematics assuming L values of 400 pc (thin discs) and 795 pc (thick disk). Using the Galactic potential in Allen & Santillan (1991) as revised by Irrgang et al. (2013), we calculate velocity in the direction of the Galactic center (V_ρ) and the Galactic rotation direction (V_ϕ), the Galactic orbital eccentricity (e), and the angular momentum in the Galactic z direction (J_z). The Galactic radial velocity V_ρ is negative toward the Galactic center, while stars that are revolving on retrograde orbits around the Galactic center have negative V_ϕ. Stars on retrograde orbits have positive J_z. Thin disk stars generally have very low eccentricities e. Population membership can be derived from the position in the V_ρ–V_ϕ diagram and the J_z–e diagram (Pauli et al. 2003, 2006). We find that for all objects the population membership is independent of the assumption for L and we apply the appropriate value for L for the distance estimation. Figure 2 shows the population memberships for our candidate LISA sources. Most systems can be identified as thin disk objects. Table 2 presents the calculated distances with the assigned value for L.

3.4. GW Parameter Estimation

Gravitational radiation for a typical stellar remnant binary at mHz frequencies can be modeled as a quasi-monochromatic signal characterized by eight parameters: GW frequency f, heliocentric amplitude $\mathcal{A}$, frequency derivative $\dot{f}$, sky coordinates (λ, β), inclination angle ι, polarization angle ψ, and initial phase ϕ_0. The GW frequency and amplitude are given by

$$f = 2/P_{\mathrm{orb}}, \tag{3}$$

with P_{orb} being the binary's orbital period, and

$$\mathcal{A} = \frac{2(G\mathcal{M})^{5/3}}{c^4 d}(\pi f)^{2/3}. \tag{4}$$

This is set by the binary's distance d and chirp mass

$$\mathcal{M} = \frac{(m_1 m_2)^{3/5}}{(m_1 + m_2)^{1/5}}, \tag{5}$$

for component masses m_1 and m_2. The frequency derivative $\dot{f}$ is expected to follow the gravitational radiation equation:

$$\dot{f} = \frac{96}{5}\frac{(G\mathcal{M})^{5/3}}{\pi c^5}(\pi f)^{11/3}. \tag{6}$$

To forecast LISA observations of the known binaries we use the VBMCMC sampler in LDASOFT (Littenberg et al. 2020). The sampler uses a parallel tempered Markov Chain Monte Carlo

---

[21] Taken from the Gaia eDR3 documentation https://gea.esac.esa.int/archive/documentation/GEDR3/Data_processing/chap_simulated/sec_cu2UM/ssec_cu2starsgal.html.
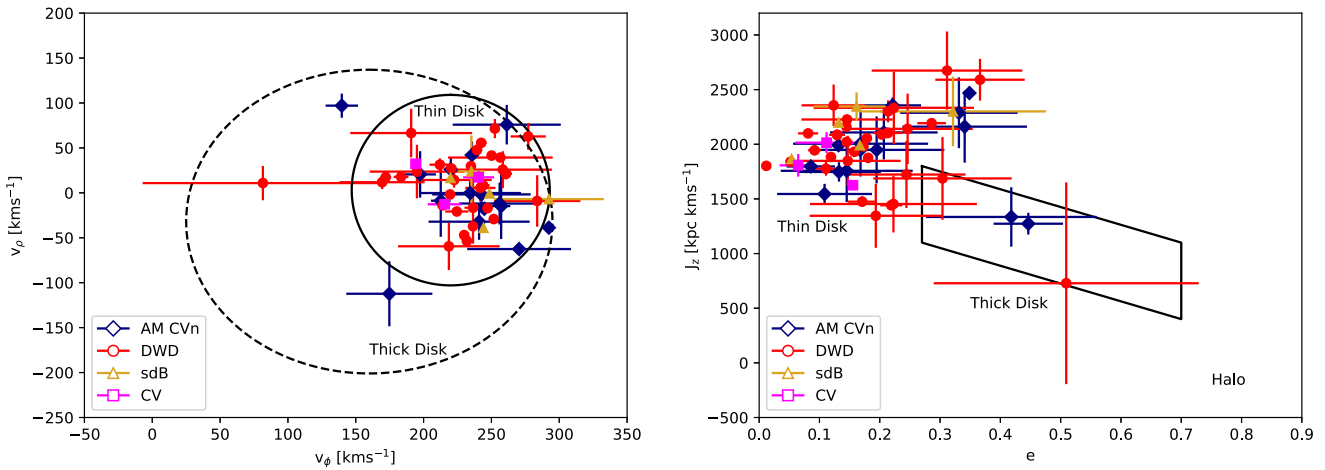
Figure 2. V_ϕ–V_ρ (left) and e–J_z diagrams (right). The solid and dotted ellipses render the 3σ thin and thick disk contours in the V_ϕ–V_ρ diagram, while the solid box in the e–J_z marks the thick disk region as specified by Pauli et al. (2006)

algorithm with delta-function priors on the orbital period and sky location of the binary based on the EM observations (see Table 1). The priors on the remaining parameters are uniform in log amplitude and cosine inclination with the start value for the inclination being set to the measured values for systems with constraints on the inclination and set to 60° for unconstrained systems. The sampler is also marginalizing over the first time derivative of the frequency, polarization angle, and initial phase of the binary, all of which are considered nuisance parameters for this study. Because this is a targeted analysis of known binaries the trans-dimensional sampling capabilities in `LDASOFT` are disabled and the algorithm uses a single template to recover the signal—effectively a delta-function prior on the model. In this configuration, results for binaries below the detection threshold are used to set upper limits on the GW amplitude parameter.

The data being analyzed are simulated internally by `VBMCMC` and include stationary Gaussian noise with the same instrument noise spectrum as was used for the LISA Data Challenges in Challenge 2a[22] plus an estimated astrophysical foreground from the unresolved Galactic binaries as described in Cornish & Robson (2017). The analysis ignores any correlations, contamination, or additional statistical uncertainty caused by the presence of other signals in the data, and also treats the astrophysical foreground as a stationary noise source. Relaxing these simplifying assumptions will be most relevant for binaries where the astrophysical foreground dominates the instrument noise spectrum at GW frequencies $\lesssim 3$ mHz but is currently beyond the scope of this analysis (considering overlap with other sources) or capabilities of the sampling algorithm (considering nonstationary noise).

4. Results

We analyze 55 verification binary candidates in total using the `VBMCMC` sampler in `LDASOFT` for increasingly longer LISA mission science operation time: 1, 3, 6, 12, 36, and 48 months. We remind the reader that we perform a *targeted* analysis by fixing— using delta-function priors—binary's sky position and orbital period to the values provided by EM measurements; additionally, we marginalize over $\dot{f}$, ψ, and ϕ_0 (see Section 3.4). Differently from our previous work to assess

the detectability of a binary, instead of evaluating the S/N we look at the binary's GW parameters posterior samples. We consider the binary as *detectable* if the GW amplitude parameter is constrained away from the minimum value allowed by the prior. This is most readily identifiable by looking at the two-dimensional posterior distribution in the GW amplitude-inclination plane, where a detectable binary will have closed contours in the posterior. We call as *verification binary* a system that becomes detectable (as explained in Section 1) within 3 months of observation time with LISA and we call as *detectable binary* when it is detected after 48 months of observation time with LISA. We introduce this distinction to highlight the use of verification binaries for the early data validations, e.g., in preparation for the first data release.

Our results show that an integration time as short as 1–3 months would allow for basic consistency tests on the recovered parameters on a few epochs of commissioning data for 9–18 verification binaries, while extending our definition up to 6 months increases the sample by only four additional binaries. To clarify the difference between a verification, detectable, and non-detectable binary, in Figure 3 we show posteriors of the binary's inclination and GW amplitude for three examples: ZTF J1539 ($\sim$7 minute orbital period, verification binary), ZTF J2029 ($\sim$21 minutes, detectable binary), and SDSS J0822 ($\sim$40 minutes, non-detectable binary). ZTF J1539 shows closed contours already after 1 month of observations, which become increasingly narrow as observation time increases. Being detectable so early on, it is highly likely that ZTF J1539 can be used as one of LISA's verification binary. ZTF J2029 represents an intermediate case as initially its posterior contours are open at low amplitude, but they close after 36 months at which point we classify this binary as detectable. Finally, we show the case of SDSS J0822, which, based on the same reasoning as above, we classify as non-detectable. The right panels of Figure 3 illustrate how LISA's fractional error on GW amplitude $\mathcal{A}$ and inclination ι (orange lines) improve over time. Assuming that EM measurement would not improve in the future, which is plausible if no additional EM measurements are taken between now and when LISA flies, we show the estimate of the same parameters based on the current EM measurement (gray lines) for comparison.

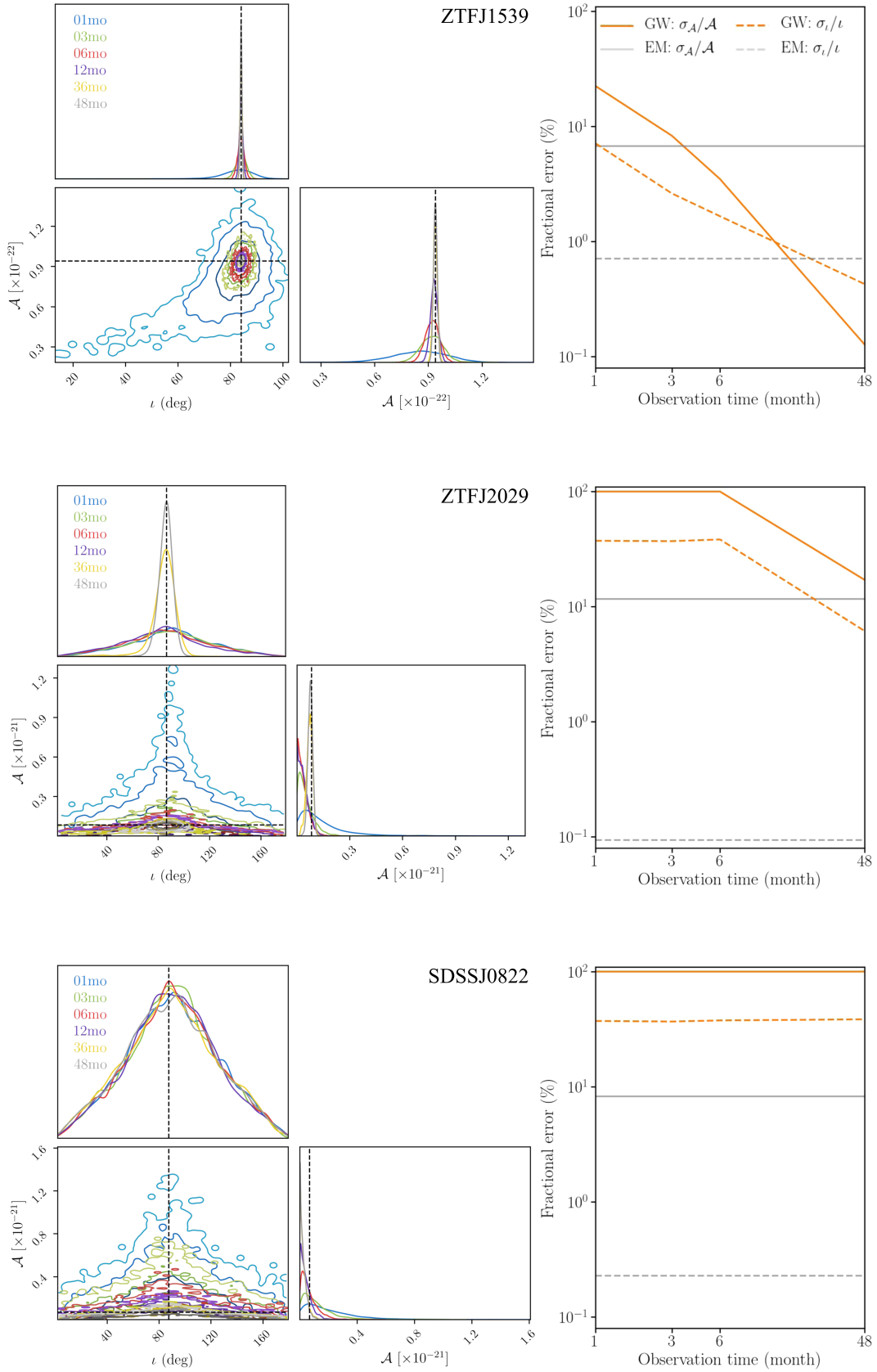**Figure 3.** Three examples of posteriors for binary's inclination and GW amplitude; from top to bottom these are ZTF J1539 (verification binary), ZTF J2029 (detectable binary), and SDSS J0822 (non-detectable binary). On the left we show how the estimated fractional error on the amplitude $\sigma_{\mathcal{A}}/\mathcal{A}$ and inclination σ_{ι}/ι change as the functions of observation time; for comparison, we also show current EM constraints and assume that these will not change before LISA's launch (see Tables 1 and 2).

Table 2
Measured EM Properties (Parallax, Distance) and Derived GW Parameters of the Verification Binaries and Detectable Binaries

Source	f (mHz)	ϖ DR3[a] (mas)	ϖ DR2[a] (mas)	L (pc)	d (pc)	$\sigma_{\mathcal{A}}/\mathcal{A}$ (%)	$\Delta\iota$ (deg)
Verification Binaries							
HM Cnc	6.220	⋯	⋯		[5000–10,000]	9.5	21
ZTF J1539	4.822	−0.4926 ± 0.5726	−0.1125 ± 0.7884	795	2469 ± 1253	1.1	0.6
ZTF J2243	3.788	−1.2372 ± 0.6578	−1.5658 ± 1.0522	400	1756 ± 726	0.36	0.6
V407 Vul	3.512	0.0978 ± 0.2384	0.0949 ± 0.3272	400	2089 ± 684	2.0	1.9
ES Cet	3.225	0.5606 ± 0.0677	0.5961 ± 0.1081	795	1779 ± 234	2.2	2.1
SDSS J0651	2.614	1.0071 ± 0.3091	1.0002 ± 0.4759	400	958 ± 370	1.8	0.9
ZTFJ 0538	2.308	0.9617 ± 0.2866	1.1477 ± 0.4811	400	999 ± 366	2.8	1.5
SDSS J1351	2.130	0.6584 ± 0.2197	0.5957 ± 0.3134	795	1530 ± 755	27.9	33
AM CVn	1.944	3.3106 ± 0.0303	3.3512 ± 0.0452	795	302 ± 3	12.5	23
ZTF J1905	1.938	1.8652 ± 1.5428	⋯	400	697 ± 605	11.6	35
SDSS J1908	1.843	1.0232 ± 0.0335	0.9542 ± 0.0464	400	977 ± 32	19.5	30
HP Lib	1.814	3.5674 ± 0.0313	3.6225 ± 0.0525	400	280 ± 3	13.3	24
SDSS 0935	1.683	2.7034 ± 0.6648	⋯	400	395 ± 203	3.3	3.1
J0526+5934	1.625	1.1826 ± 0.0910	1.1294 ± 0.1097	400	845 ± 68	18.0	9.6
J1239-2041	1.481	1.0068 ± 0.2309	1.4054 ± 0.3297	400	972 ± 272	13.3	9.5
TIC 378898110	1.483	3.2328 ± 0.0195	3.2186 ± 0.0307	400	309 ± 2	⋯	⋯
CR Boo	1.359	2.8438 ± 0.0367	⋯	400	351 ± 5	19.8	29
SDSS J0634	1.257	2.3111 ± 0.0835	2.3578 ± 0.091	400	433 ± 16	19.4	28
V803 Cen	1.253	3.4885 ± 0.0599	⋯	400	287 ± 5	16.1	27
Detectable Binaries							
4U 1820-30	2.920	−0.7676 ± 0.2164	−0.8199 ± 0.2065	⋯	7972±277[c]	32.3	34
ZTF J0127	2.431	0.4438 ± 0.4657	⋯	400	1283 ± 603	7.2	2.4
SDSS J2322	1.665	1.1558 ± 0.2244	1.2869 ± 0.2830	400	859 ± 206	29.6	36
PTF J0533	1.621	0.7902 ± 0.2396	0.4741 ± 0.4786	400	1173 ± 390	33.3	30
ZTF J2029	1.597	0.1240 ± 0.9893	−1.4269 ± 1.4345	400	1095 ± 644	18.4	10
PTF 1J1919	1.484	0.6229 ± 0.2385	0.5499 ± 0.3274	400	1364 ± 471	65.2	46
TIC 378898110	1.484	3.2328 ± 0.0195	3.2186 ± 0.0307	400	309 ± 2	19.0	6.5
CXOGBS J1751	1.456	0.8591 ± 0.1733	0.4994 ± 0.2130	400	1128 ± 258	48.4	41
ZTF J0722	1.406	0.6996 ± 0.2457	0.4132 ± 0.3508	795	1461 ± 785	46.3	23
KL Dra	1.332	1.0817 ± 0.0989	1.0354 ± 0.1488	795	930 ± 91	65.4	49
PTF 1J0719	1.245	1.1851 ± 0.2292	1.1436 ± 0.3009	400	840 ± 201	68.0	48
CP Eri	1.149	1.3451 ± 0.2759	0.6836 ± 0.9407	400	747 ± 203	82.6	55
SMSS J0338	1.089	1.8675 ± 0.0562	1.8994 ± 0.0793	400	536 ± 16	43.2	40
J2322+2103	1.043	0.8261 ± 0.2503	0.6943 ± 0.3168	400	1134 ± 386	38.1	38
SDSS J0106	0.853	1.2011 ± 0.4739	1.3521 ± 0.5726	400	824 ± 441	76.7	51
SDSS J1630	0.837	1.1748 ± 0.1952	0.9366 ± 0.2704	400	848 ± 167	40.1	39
J1526m2711	0.827	1.6053 ± 0.1751	1.5683 ± 0.2203	400	625 ± 75	39.8	38
SDSS J1235	0.673	2.2504 ± 0.1389	2.3319 ± 0.1660	400	446 ± 28	39.8	38
SDSS J0923	0.515	3.4795 ± 0.0648	3.3397 ± 0.1052	400	288 ± 5	41.3	38
CD-30 11223	0.473	2.8198 ± 0.0516	2.9629 ± 0.0797	400	355 ± 7	67.8	46
SDSS J1337	0.337	8.8007 ± 0.0440	8.6993 ± 0.0524	400	114 ± 1	32.1	35
HD 265435	0.336	2.1666 ± 0.0554	2.1994 ± 0.0628	400	461 ± 12	70.6	54

Notes. The distance for HM Cnc is assumed. The fractional error for the amplitude ($\sigma_{\mathcal{A}}/\mathcal{A}$) and the precision of the inclination ($\Delta\iota$) is calculated for 4 yr integration with LISA.
[a] Gaia Collaboration et al. (2018).
[b] Gaia Collaboration et al. (2021).
[c] Baumgardt & Vasiliev (2021).

Based on our definition above, overall we find 40 binaries detectable with LISA within 4 yr of science operations, out of which we classify 18 (10 AM CVns + eight DWDs) as verification binaries, i.e., detectable within the first 3 months. We list their properties in Tables 1 and 2. The summary of our results is presented in Figure 4. In the left panel, we show a characteristic strain–frequency plot for all detectable binaries: AM CVns in blue, DWDs in red, sdBs in yellow, and UCXB in magenta. Filled stars represent LISA verification binaries, and empty stars are detectable binaries within the nominal mission lifetime (48 months). We compute the error bars on a

characteristic strain by generating random samples from EM measurement uncertainties on binary component masses and distance (see Tables 1 and 2); in the figure, we plot a 1σ uncertainty based on our random samples. For comparison, we also show a mock Galactic DWD population of Wilhelm et al. (2021) in gray, as well as the LISA sensitivity curve at S/N = 6 as a black solid line. The comparison reveals that the current sample of known binaries is mainly representative of the *loudest* GW sources in the Milky Way, while the majority is yet to be discovered in more remote parts of our Galaxy inaccessible for EM observatories (see Figure 15 of
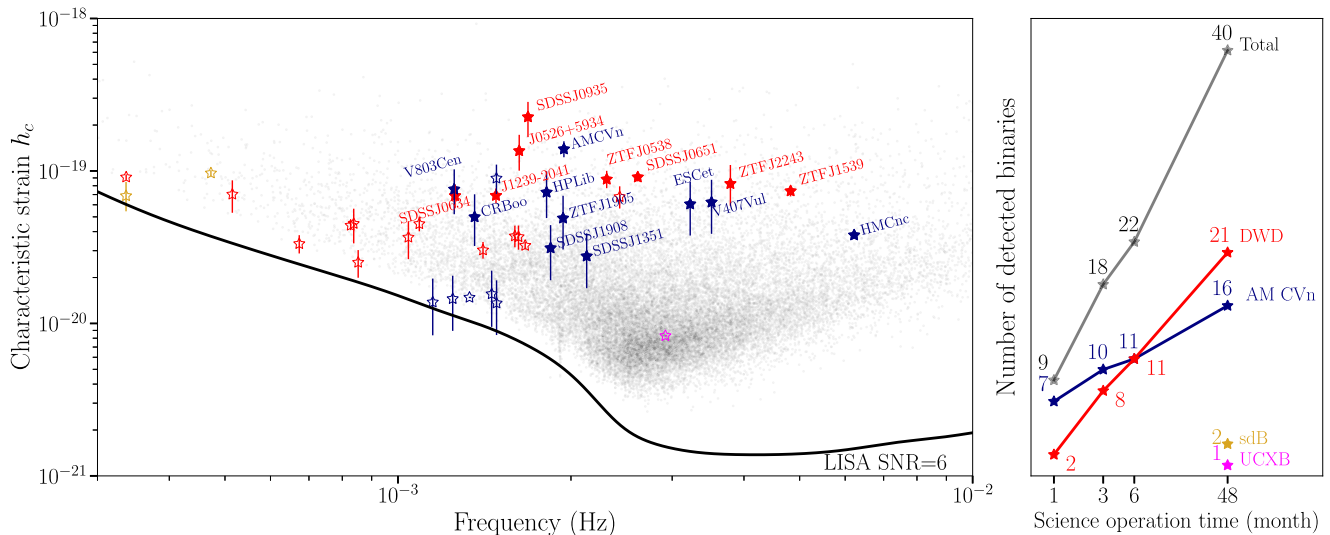
Figure 4. Left panel: characteristic strain–frequency plot for detectable and verification binaries: AM CVns in blue, DWDs in red, sdBs in yellow, and UCXB in magenta. Filled stars represent binaries detectable within 3 months of observations, which here we call verification binaries. The error bars on characteristic strain show 1σ uncertainty evaluated by generating random samples from EM measurement uncertainties on binary component masses and distances presented in Tables 1 and 2. The black solid line represents LISA's sensitivity curve that accounts for the instrumental noise (LISA Science Study Team 2018) and Galactic confusion foreground (Babak et al. 2017). For comparison in gray, we show a mock Galactic DWD population detectable with LISA from Wilhelm et al. (2021). Right panel: number of detected binaries as a function of science operation time.

Amaro-Seoane et al. 2023). In the right panel of Figure 4, we show the detection statistic as a function of the science operation time with a breakdown for different types of binaries showing that increased science operation for LISA will lead to a larger number of detected binaries in the LISA data. We note that in our study none of the CVs will be detectable within 4 yr of LISA observations.

In our previous study Kupfer et al. (2018), we identified 13 detectable binaries. The reasons for the difference are multiple. First, the sample of candidate verification binaries has tripled in the past few years (see Section 2). Second, some distance estimates have improved between Gaia DR2 and DR3 (this is, for example, true for CXOGBS J1751 and SDSSJ163); for some binaries (ZTF J0127, ZTF J1905, SDSS J0935, V803 Cen, CR Boo) parallaxes were not available as part of the DR2. Most importantly, we also change our criterion for the detectability moving away from an S/N-based definition. Recently, Finch et al. (2023) have used our catalog for a number of LISA data analysis investigations by performing a Bayesian parameter estimation with the `BALROG` code (Roebber et al. 2020; Buscicchio et al. 2021; Klein et al. 2022). They verified that binaries with S/N < 6 generally display broad posteriors, with no clear peaks and with amplitude parameters being inconsistent with zero. Thus, they adopted the S/N threshold of 6 as the criterion for the detectability with LISA. They found that up to 14 binaries can be detected within 3 months of observations (see their Figures 4 and B1). This result is in agreement with ours considering new binaries that have been added to the list of candidates in our study.

We report the estimated fractional error on the GW amplitude ($\sigma_A/\mathcal{A}$) and the estimated precision for the inclination ($\Delta\iota$) that can be reached after 4 yr of observation in Table 2. On average, for verification binaries, the amplitude is forecasted to be measured at $\sim$10%, while the inclination is expected to be determined with $\sim$15° precision. For detectable binaries, these average errors decrease to $\sim$50% and $\sim$40°, respectively. From the table, one can deduce that the

measurements depend on the binary's frequency (generally improving with increasing frequency) and the strength of the signal (with verification binaries being better characterized than detectable binaries). Our estimates are in good agreement with (Finch et al. 2023, see their Table 2).

Figures 5 and 6 illustrate, respectively, the position of detectable (empty symbols) and verification (filled symbols) binaries on the sky and on the Gaia Hertzsprung–Russell (H-R) diagram. Both reveal different limitations of the current sample. Figure 5 shows that although the size of the candidate LISA binaries is progressively growing, it is still biased toward the Northern Hemisphere (where the majority of surveys have been conducted so far), and to high latitudes (to avoid the dust extinction and crowding in the Galactic plane). From observations of bright nondegenerate stars, we know that the Galactic stellar population is concentrated in the disk (the region in between the dashed lines) peaking toward the Galactic center (thick black cross in Figure 5), and so we expect LISA detectable binaries to follow the same distribution (e.g., see Szekerczes et al. 2023). Figure 6 shows our sample of LISA sources compared to the absolute magnitudes (M_G) and colors ($BP - RP$) of Gaia's sample of stars with parallax uncertainty below 1% (gray points). The plot shows a bias toward sources brighter and bluer compared to objects on the white dwarf track where most DWDs are expected. We note that on the H-R diagram, we use downward-pointing triangles to highlight that our absolute magnitude estimates in our sample are to be interpreted as upper limits. This is because for all candidate LISA binaries the extinction, which is necessary to convert apparent G magnitudes measured by Gaia magnitudes into absolute magnitudes M_G, is not well measured. Potential LISA sources with larger magnitudes can only be observed up to a couple of kiloparsecs with current surveys, which limits the volume where LISA binaries can be detected. In contrast to EM searches, LISA measures directly the amplitude of GW waves, rather than the energy flux. Thus, the observed GW signal scales as $1/d$, rather than $1/d^2$, allowing LISA to detect binaries at larger distances—potentially within
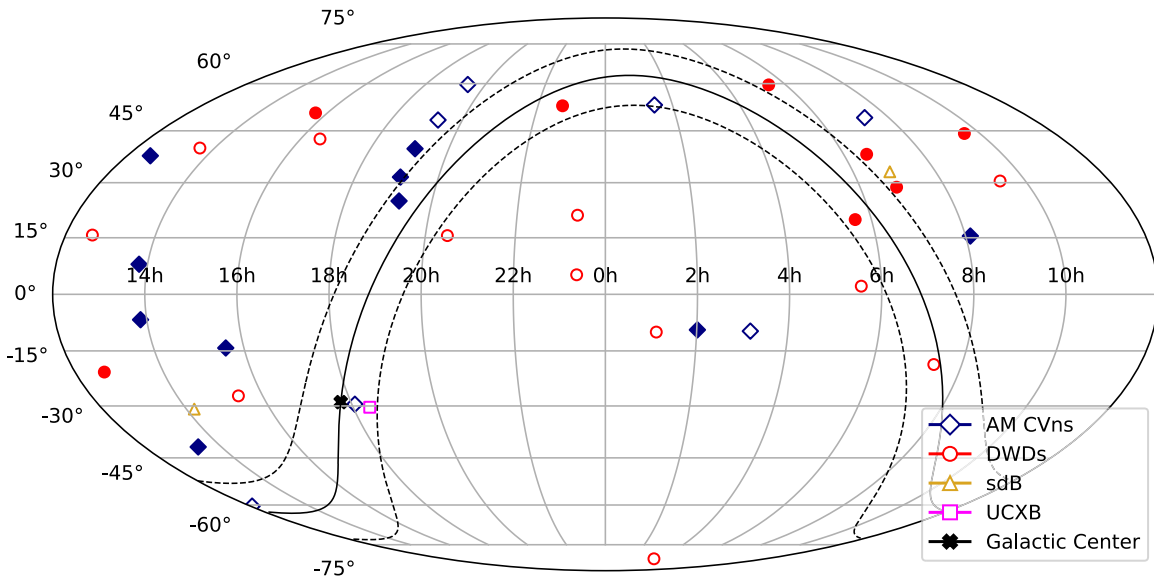
Figure 5. The position of the LISA binaries on the sky in an equatorial projection, with the Galactic plane (±10°) shown by the solid and dashed lines. Filled symbols are verification binaries, whereas open symbols are detectable binaries.

the entire Milky Way volume—than in the traditional EM observational bands.

5. Discussion

5.1. Limitations of the Current Sample and Prospects to Expand the Sample

The currently known sample of candidate LISA verification binaries is inhomogeneous and biased. This bias is evident in the sky distribution (Figure 5), predominantly favoring the Northern Hemisphere with 60% of LISA sources. Furthermore, the H-R diagram (Figure 6) reveals an overrepresentation of sources above the main white dwarf track. This is due to the nature of volume-limited ground-based surveys favoring brighter sources. Finally, a significant challenge lies in the multitude of detection and analysis methods, leading to a nonuniformity in presenting parameters of these binaries. Parameters are presented in varied ways: with a 1σ error, no constraints, approximations, or limits. To facilitate more effective future multi-messenger studies, it is essential to develop uniform analysis methods that provide a standard set of prior information.

Between Gaia DR2 and Gaia DR3, the number of detectable LISA sources has tripled, which can be explained by the large number of sky surveys that have come online over the last few years. This will improve even more over the next decade with many additional surveys coming online over the next few years. As proven in the past, photometric and spectroscopic surveys are ideal tools to find new LISA binaries and complement each other. Eclipses or tidal deformation lead to photometric variability on the orbital period, whereas compact LISA binaries show up in multi-epoch spectroscopy due to large radial velocity shifts between individual spectra.

SDSS-V is an all-sky, multi-epoch spectroscopic survey that started operations in 2020 and will provide spectra for a few million sources (Kollmeier et al. 2017). Already in early SDSS-V data, Chandra et al. (2021) discovered a new detectable LISA binary. Other spectroscopic ongoing or upcoming spectroscopic surveys include LAMOST (Zhao et al. 2012),

4MOST (de Jong et al. 2019), or WEAVE (Dalton et al. 2014). The Asteroid Terrestrial-impact Last Alert System (Heinze et al. 2018; Tonry et al. 2018) and the Gravitational-wave Optical Transient Observer (Steeghs et al. 2022) are ongoing photometric sky surveys with telescopes located in both hemispheres allowing for an all-sky coverage for both surveys. Their cadence and sky coverage are well suited to find LISA detectable binaries. BlackGEM is a photometric sky survey covering the Southern Hemisphere, which started operations in 2023 (Bloemen et al. 2015). Part of the BlackGEM operations will be the BlackGEM Fast Synoptic Survey, which is a continuous high-cadence survey of individual fields in the Southern Hemisphere. The cadence is ideal to discover new LISA detectable binaries. First light for the Vera Rubin telescope is expected in 2024. The telescope will perform the Legacy Survey of Space and Time (LSST) covering the Southern Hemisphere down to 24 mag (per single exposure) going much deeper and hence covering a significantly larger volume than current sky surveys. Although the cadence is expected to be not ideal for LISA binaries, LSST will collect sufficient photometric observations over 10 yr to be able to discover LISA binaries. The next large Gaia data release (DR4) is expected to include precision time-series photometry of ≈70 epochs for each object taken over a 5 yr time frame. Euclid is a space mission operating in the near-infrared and visible bands, which was launched in 2023 with an unprecedented sky resolution of almost 1 order of magnitude better compared to ground-based observatories. Part of Euclid's operation will be the Euclid deep survey covering a total of 40 sqd for three distinct fields. Each field will get several tens of epochs over its nominal mission time of 6 yr with a depth of ≈25 mag for each epoch in the near-infrared bands (Laureijs et al. 2011). Finally, in the late 2020s, the Nancy Roman space telescope will conduct a wide-field survey with the same sky resolution as Euclid down to 24 mag. Therefore, we expect that the number of LISA detectable sources will significantly increase before the LISA launches providing a large sample of multi-messenger sources (e.g., Korol et al. 2017; Li et al. 2020).
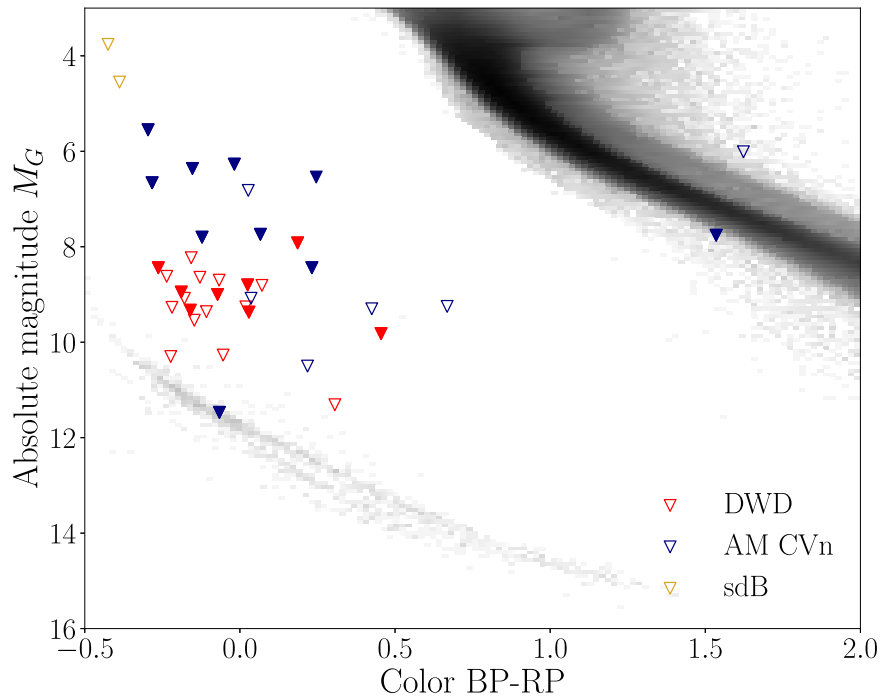
Figure 6. Verification binaries (in color) on the Gaia H-R diagram (in gray). Downward-pointing triangles are used to symbolize that absolute magnitude estimates are to be interpreted as upper limits because we do not account for extinction. As before, filled symbols represent verification binaries, whereas open symbols represent detectable binaries.

5.2. Focus on Future EM Efforts

EM measurement of a binary's inclination will significantly inform LISA's data analysis and parameter estimation, particularly for nearly edge-on systems (Table 1). As Shah et al. (2012) outlined, EM inclination data enhances GW amplitude measurement due to the strong correlation between amplitude and inclination parameters in GW data (Figure 3). This improves chirp mass and distance determination. Also, Finch et al. (2023) demonstrated the advantage of EM prior information in reducing detection time versus a blind search. They show that after the binary has been detected, further parameter estimation improvements are inclination dependent; face-on sources benefit greatly from prior inclination knowledge, with amplitude measurement improvement increasing with observation time (see their Figure 5). This underscores the importance of binary inclination data from EM observations for future LISA data analysis. However, 40% of current sources lack inclination measurement. These are primarily non-eclipsing sources where measurement is nontrivial.

Determining $\dot{f}$ from GW data alone can be challenging for low-frequency ($f < 2$ mHz) and/or low-S/N binaries. On the other hand, high-precision $\dot{f}$ measurement is achievable via EM observations for eclipsing sources through ground-based eclipse timing measurements over long baselines (e.g., >10 yr). Shah & Nelemans (2014) demonstrated the accuracy improvement in the chirp mass when adding EM $\dot{f}$ data to GW analysis.

Knowledge of distance (d) or parallax (ϖ) is also crucial for characterizing LISA binaries. As mentioned in Section 3.3, parallax constrains the luminosity distance, directly affecting GW amplitude (Equation (4)). LISA's GW frequency and amplitude measurements, coupled with Gaia-based parallax, allow binary chirp mass determination (solving Equation (4) for $\mathcal{M}$) without measuring $\dot{f}$, usually required for chirp mass

determination from GW data (Equation (6)). Error propagation illustrates that chirp mass error and parallax error are linearly related ($\sigma_{\mathcal{M}}/\mathcal{M} \propto \varpi\sigma_{\varpi}$), meaning that parallax measurement improvement directly enhances chirp mass estimation. This method recovers chirp masses for binaries at LISA's low-frequency end and for interacting binaries, whose $\dot{f}$ contains an astrophysical contribution (e.g., Breivik et al. 2018; Littenberg & Cornish 2019), as in verification binaries AM CVn and HP Lib.

The forthcoming Gaia DR4, based on 66 months of data collection, should mark a significant improvement over DR3 (34 months). An estimated improvement factor for parallax errors of ∼0.7 can be expected (using $\sigma_{\varpi} \propto (T_{DR3}/T_{DR4})^{0.5} \sim (34/66)^{0.5}$), with T_{DR3} and T_{DR4} expressed in months, see Gaia Collaboration et al. (2018). Additional enhancements in Gaia data quality are anticipated, given the indicative mission extension until 2025,[23] allowing for data collection up to a total of 10 yr. However, very distant or faint systems might never have a reliable parallax measurement from Gaia. If the period is sufficiently short, LISA will provide an $\dot{f}$ measurement that can break the degeneracy between chirp mass and distance, and as such, LISA will provide an independent distance measurement. Figure 7 shows the expected distance measurement from LISA for HM Cnc. We expect an uncertainty of about 1.5–2 kpc, which is significantly better than any current estimates from EM observations (see Section 3.2).

6. Summary and Conclusions

In this work, we derive updated distances and kinematics for 55 verification binary candidates using parallaxes and proper motions from Gaia DR3. Using these distances and system properties we calculate the detectability for each source after 1,
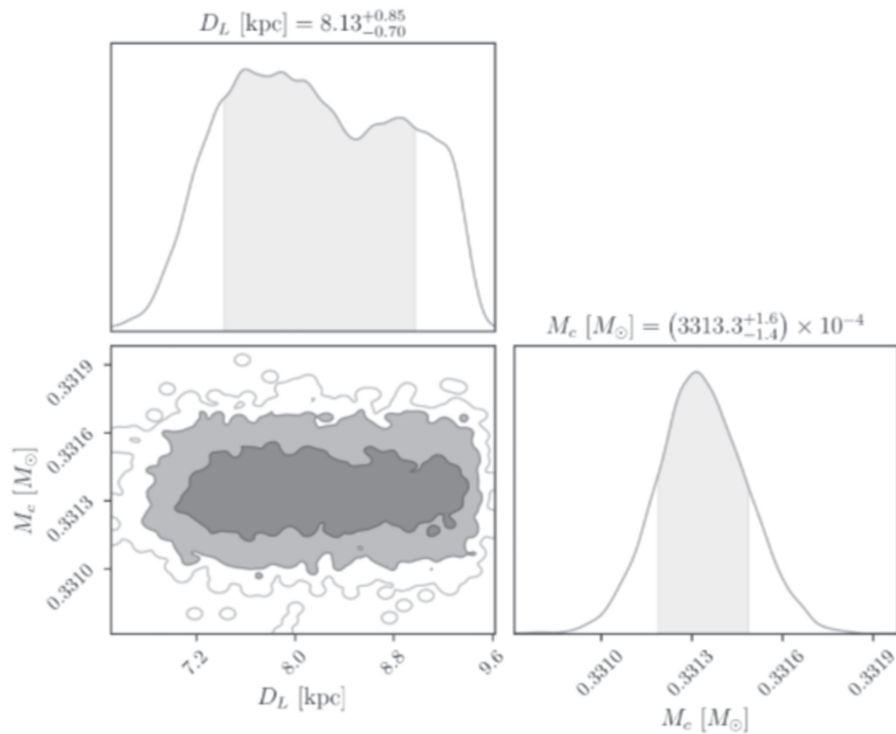

Figure 7. Posterior distribution for HM Cnc's expected chirp mass and distance precision predicted for four years of LISA observations.

3, 6, and 48 months of LISA observations. We find that 18 verification binaries can be detected after 3 months of LISA observations and used for science verification. An additional 22 sources will be detected after 48 months of LISA observations totaling the number of detectable LISA to a total of 40 sources. The sources consist of 21 DWDs, 16 AM CVn binaries, two hot subdwarf binaries, and one ultracompact X-ray binary. In particular, AM CVn and HP Lib are verification binaries with parallax errors below 1% making them ideal validation sources.

The number of detectable LISA binaries has tripled over the last 5 yr since Kupfer et al. (2018). That is mainly due to the increasing number of large-scale sky surveys, in particular, the ELM survey and ZTF were driving the discoveries over the last few years. However, even with the large increase in sources, the sample is still strongly biased toward luminous binaries and sources located in the Northern Hemisphere. However, we predict that the number of systems will continue to increase significantly over the next few years with additional large-scale surveys coming online over the next few years and strategies need to be developed to perform efficient follow-up for each source before LISA launches.

For sources without a measured $\dot{f}$, generally, the distance is required to measure the chirp mass. The error on the parallax scales linearly with the error on the chirp mass. We find that the parallax precision has improved by 20%–30% between Gaia DR2 and DR3 and another $\approx$30% improvement is expected for Gaia DR4. We find that on average for verification binaries the GW amplitude is expected to be measured to $\approx$10% precision, while the inclination is expected to be determined with $\approx$15° precision. For detectable binaries, these average errors decrease to $\approx$50% and $\approx$40°, respectively. At present, 40% of the LISA sources have no measured inclination from EM observations. These are mainly non-eclipsing sources where it is nontrivial to measure an inclination angle and it might be that no progress will be made on the inclination before LISA. Therefore, even

an uncertain inclination measurement from LISA will be extremely valuable.

Properties for all sources collected for this publication are publicly available on the LISA Consortium GitLab repository https://gitlab.in2p3.fr/LISA/lisa-verification-binaries. We wish to keep this list up to date for the Consortium and the broader community. Thus, we welcome submission requests for new binaries and/or other suggestions.

ORCID iDs

Thomas Kupfer ⓘ https://orcid.org/0000-0002-6540-1484
Valeriya Korol ⓘ https://orcid.org/0000-0002-6725-5935
Tyson B. Littenberg ⓘ https://orcid.org/0000-0002-9574-578X
Sweta Shah ⓘ https://orcid.org/0000-0002-0716-1320
Etienne Savalle ⓘ https://orcid.org/0000-0001-6201-0560
Thomas R. Marsh ⓘ https://orcid.org/0000-0002-2498-7589
Anna F. Pala ⓘ https://orcid.org/0000-0001-7069-7403
Antoine Petiteau ⓘ https://orcid.org/0000-0002-7371-9695
Gavin Ramsay ⓘ https://orcid.org/0000-0001-8722-9710
Danny Steeghs ⓘ https://orcid.org/0000-0003-0771-4746

References

Allen, C., & Santillan, A. 1991, RMxAA, 22, 255
Amaro-Seoane, P., Andrews, J., Arca Sedda, M., et al. 2023, LRR, 26, 2
Amaro-Seoane, P., Audley, H., Babak, S., et al. 2017, arXiv:1702.00786
Anderson, S. F., Haggard, D., Homer, L., et al. 2005, AJ, 130, 2230
Astraatmadja, T. L., & Bailer-Jones, C. A. L. 2016, ApJ, 832, 137
Astropy Collaboration, Price-Whelan, A. M., Sipőcz, B. M., et al. 2018, AJ, 156, 123
Astropy Collaboration, Robitaille, T. P., Tollerud, E. J., et al. 2013, A&A, 558, A33
Babak, S., Gair, J., Sesana, A., et al. 2017, PhRv, D95, 103012
Bailer-Jones, C. A. L. 2015, PASP, 127, 994
Bailer-Jones, C. A. L., Rybizki, J., Fouesneau, M., Mantelet, G., & Andrae, R. 2018, AJ, 156, 58
Bailer-Jones, C. A. L., Rybizki, J., Fouesneau, M., Demleitner, M., & Andrae, R. 2021, AJ, 161, 147
Baumgardt, H., & Vasiliev, E. 2021, MNRAS, 505, 5957
Bellm, E. 2014, in The Third Hot-wiring the Transient Universe Workshop, ed. P. R. Wozniak et al., 27, www.slac.stanford.edu/econf/C131113.1/
Belokurov, V., Penoyre, Z., Oh, S., et al. 2020, MNRAS, 496, 1922
Bloemen, S., Groot, P., Nelemans, G., & Klein-Wolt, M. 2015, in ASP Conf. Ser. 496, Living Together: Planets, Host Stars and Binaries, ed. S. M. Rucinski, G. Torres, & M. Zejda (San Francisco, CA: ASP), 254
Breedt, E., Steeghs, D., Marsh, T. R., et al. 2017, MNRAS, 468, 2910
Breivik, K., Coughlin, S., Zevin, M., et al. 2020, ApJ, 898, 71
Breivik, K., Kremer, K., Bueno, M., et al. 2018, ApJL, 854, L1
Brown, W. R., Gianninas, A., Kilic, M., Kenyon, S. J., & Allende Prieto, C. 2016a, ApJ, 818, 155
Brown, W. R., Kilic, M., Allende Prieto, C., & Kenyon, S. J. 2010, ApJ, 723, 1072
Brown, W. R., Kilic, M., Bédard, A., Kosakowski, A., & Bergeron, P. 2020, ApJL, 892, L35
Brown, W. R., Kilic, M., Hermes, J. J., et al. 2011, ApJL, 737, L23
Brown, W. R., Kilic, M., Kenyon, S. J., & Gianninas, A. 2016b, ApJ, 824, 46
Brown, W. R., Kilic, M., Kosakowski, A., & Gianninas, A. 2022, ApJ, 933, 94
Burdge, K. B., Coughlin, M. W., Fuller, J., et al. 2019a, Natur, 571, 528
Burdge, K. B., Coughlin, M. W., Fuller, J., et al. 2020b, ApJL, 905, L7
Burdge, K. B., El-Badry, K., Rappaport, S., et al. 2023, ApJL, 953, L1
Burdge, K. B., Fuller, J., Phinney, E. S., et al. 2019a, ApJL, 886, L12
Burdge, K. B., Prince, T. A., Fuller, J., et al. 2020b, ApJ, 905, 32
Buscicchio, R., Klein, A., Roebber, E., et al. 2021, PhRvD, 104, 044065
Chandra, V., Hwang, H.-C., Zakamska, N. L., et al. 2021, ApJ, 921, 160
Chen, W.-C., Liu, D.-D., & Wang, B. 2020, ApJL, 900, L8
Cornish, N., & Robson, T. 2017, JPhCS, 840, 012024
Dalton, G., Trager, S., Abrams, D. C., et al. 2014, Proc. SPIE, 9147, 91470L
de Jong, R. S., Agertz, O., Berbel, A. A., et al. 2019, Msngr, 175, 3
Espaillat, C., Patterson, J., Warner, B., & Woudt, P. 2005, PASP, 117, 189
Finch, E., Bartolucci, G., Chucherko, D., et al. 2023, MNRAS, 522, 5358
Fontaine, G., Brassard, P., Green, E. M., et al. 2011, ApJ, 726, 92
Gaia Collaboration, Brown, A. G. A., Vallenari, A., et al. 2018, A&A, 616, A1
Gaia Collaboration, Brown, A. G. A., Vallenari, A., et al. 2021, A&A, 649, A1
Gaia Collaboration, Prusti, T., de Bruijne, J. H. J., et al. 2016, A&A, 595, A1
Gaia Collaboration, Vallenari, A., Brown, A. G. A., et al. 2023, A&A, 674, A1
Geier, S., Marsh, T. R., Wang, B., et al. 2013, A&A, 554, A54
Green, G. M., Schlafly, E., Zucker, C., Speagle, J. S., & Finkbeiner, D. 2019, ApJ, 887, 93
Green, G. M., Schlafly, E. F., Finkbeiner, D., et al. 2018, MNRAS, 478, 651
Green, M. J., Hermes, J. J., Barlow, B. N., et al. 2024, MNRAS, 527, 3445
Groot, P. J., Nelemans, G., Steeghs, D., & Marsh, T. R. 2001, ApJL, 558, L123
Harms, J., Ambrosino, F., Angelini, L., et al. 2021, ApJ, 910, 1
Heinze, A. N., Tonry, J. L., Denneau, L., et al. 2018, AJ, 156, 241
Hermes, J. J., Kilic, M., Brown, W. R., et al. 2012, ApJL, 757, L21
Howell, S. B., Szkody, P., Kreidl, T. J., & Dobrzycka, D. 1991, PASP, 103, 300
Huang, S.-J., Hu, Y.-M., Korol, V., et al. 2020, PhRvD, 102, 063021
Hunter, J. D. 2007, CSE, 9, 90
Igoshev, A., Verbunt, F., & Cator, E. 2016, A&A, 591, A123
Irrgang, A., Wilcox, B., Tucker, E., & Schiefelbein, L. 2013, A&A, 549, A137
Kilic, M., Brown, W. R., Bédard, A., & Kosakowski, A. 2021, ApJL, 918, L14
Kilic, M., Brown, W. R., Gianninas, A., et al. 2014, MNRAS, 444, L1
Kilic, M., Brown, W. R., Gianninas, A., et al. 2017, MNRAS, 471, 4218
Kilic, M., Brown, W. R., Hermes, J. J., et al. 2011a, MNRAS, 418, L157
Kilic, M., Brown, W. R., Kenyon, S. J., et al. 2011b, MNRAS, 413, L101
Klein, A., Pratten, G., Buscicchio, R., et al. 2022, arXiv:2204.03423
Kollmeier, J. A., Zasowski, G., Rix, H.-W., et al. 2017, arXiv:1711.03234
Korol, V., Hallakoun, N., Toonen, S., & Karnesis, N. 2022, MNRAS, 511, 5936
Korol, V., Igoshev, A. P., Toonen, S., et al. 2023, arXiv:2310.06559
Korol, V., Rossi, E. M., Groot, P. J., et al. 2017, MNRAS, 470, 1894
Kosakowski, A., Brown, W. R., Kilic, M., et al. 2023a, ApJ, 950, 141
Kosakowski, A., Kilic, M., & Brown, W. 2021, MNRAS, 500, 5098
Kosakowski, A., Kilic, M., Brown, W. R., & Gianninas, A. 2020, ApJ, 894, 53
Kosakowski, A., Kupfer, T., Bergeron, P., & Littenberg, T. B. 2023b, ApJ, 959, 114
Kupfer, T., Bauer, E. B., Burdge, K. B., et al. 2020a, ApJL, 898, L25
Kupfer, T., Bauer, E. B., Marsh, T. R., et al. 2020b, ApJ, 891, 45
Kupfer, T., Bauer, E. B., van Roestel, J., et al. 2022, ApJL, 925, L12
Kupfer, T., Groot, P. J., Bloemen, S., et al. 2015, MNRAS, 453, 483
Kupfer, T., Korol, V., Shah, S., et al. 2018, MNRAS, 480, 302
Kupfer, T., Prince, T. A., van Roestel, J., et al. 2021, MNRAS, 505, 1254
Lamberts, A., Blunt, S., Littenberg, T. B., et al. 2019, MNRAS, 490, 5888
Laureijs, R., Amiaux, J., Arduini, S., et al. 2011, arXiv:1110.3193
Levitan, D., Fulton, B. J., Groot, P. J., et al. 2011, ApJ, 739, 68
Levitan, D., Kupfer, T., Groot, P. J., et al. 2014, ApJ, 785, 114
Li, Z., Chen, X., Chen, H.-L., et al. 2020, ApJ, 893, 2
Lindegren, L., Hernandez, J., Bombrun, A., et al. 2018, A&A, 616, A2
LISA Science Study Team 2018, LISA Science Requirements Document, Tech. Rep. ESA-L3-EST-SCI-RS-001, ES, www.cosmos.esa.int/web/lisa/lisa-documents/
Littenberg, T. B. 2018, PhRvD, 98, 043008
Littenberg, T. B., & Cornish, N. J. 2019, ApJL, 881, L43
Littenberg, T. B., & Cornish, N. J. 2023, PhRvD, 107, 063004
Littenberg, T. B., Cornish, N. J., Lackeos, K., & Robson, T. 2020, PhRvD, 101, 123021
Luo, J., Chen, L.-S., Duan, H.-Z., et al. 2016, CQGra, 33, 035010
Luri, X., Brown, A. G. A., Sarro, L. M., et al. 2018, A&A, 616, A9
Lyne, A. G., Burgay, M., Kramer, M., et al. 2004, Sci, 303, 1153
Marsh, T. R. 2011, CQGra, 28, 094019
Munday, J., Marsh, T. R., Hollands, M., et al. 2023, MNRAS, 518, 5123
Nelemans, G., & Jonker, P. G. 2010, NewAR, 54, 87
Nelemans, G., Portegies Zwart, S. F., Verbunt, F., & Yungelson, L. R. 2001, A&A, 368, 939
Nelemans, G., Yungelson, L. R., & Portegies Zwart, S. F. 2004, MNRAS, 349, 181
Nissanke, S., Vallisneri, M., Nelemans, G., & Prince, T. A. 2012, ApJ, 758, 131
Oliphant, T. E. 2015, Guide to NumPy (2nd ed.; USA: CreateSpace Independent Publishing Platform)
Patterson, J., Fried, R. E., Rea, R., et al. 2002, PASP, 114, 65
Pauli, E. M., Napiwotzki, R., Altmann, M., et al. 2003, A&A, 400, 877

Pauli, E.-M., Napiwotzki, R., Heber, U., Altmann, M., & Odenkirchen, M. 2006, A&A, 447, 173

Pelisoli, I., Neunteufel, P., Geier, S., et al. 2021, NatAs, 5, 1052

Penoyre, Z., Belokurov, V., Wyn Evans, N., Everall, A., & Koposov, S. E. 2020, MNRAS, 495, 321

Petiteau, A. 2008, PhD thesis, Univ. Paris-Diderot—Paris VII

Provencal, J. L., Winget, D. E., Nather, R. E., et al. 1997, ApJ, 480, 383

Ramsay, G., Green, M. J., Marsh, T. R., et al. 2018, A&A, 620, A141

Ramsay, G., & Hakala, P. 2002, MNRAS, 332, L7

Reinsch, K., Steiper, J., & Dreizler, S. 2007, in ASP Conf. Ser. 372, 15th European Workshop on White Dwarfs, ed. R. Napiwotzki & M. R. Burleigh (San Francisco, CA: ASP), 419

Roebber, E., Buscicchio, R., Vecchio, A., et al. 2020, ApJL, 894, L15

Roelofs, G. H. A., Groot, P. J., Benedict, G. F., et al. 2007, ApJ, 666, 1174

Roelofs, G. H. A., Groot, P. J., Marsh, T. R., Steeghs, D., & Nelemans, G. 2006, MNRAS, 365, 1109

Roelofs, G. H. A., Rau, A., Marsh, T. R., et al. 2010, ApJL, 711, L138

Ruan, W.-H., Guo, Z.-K., Cai, R.-G., & Zhang, Y.-Z. 2018, arXiv:1807.09495

Ruiter, A. J., Belczynski, K., Benacquista, M., & Holley-Bockelmann, K. 2009, ApJ, 693, 383

Savalle, E., Gair, J., Speri, L., & Babak, S. 2022, PhRvD, 106, 022003

Scaringi, S., Breivik, K., Littenberg, T. B., et al. 2023, MNRAS, 525, L50

Shah, S., & Nelemans, G. 2014, ApJ, 790, 161

Shah, S., van der Sluys, M., & Nelemans, G. 2012, A&A, 544, A153

Skillman, D. R., Patterson, J., Kemp, J., et al. 1999, PASP, 111, 1281

Solheim, J. E. 2010, PASP, 122, 1133

Steeghs, D., Galloway, D. K., Ackley, K., et al. 2022, MNRAS, 511, 2405

Steeghs, D., Marsh, T. R., Barros, S. C. C., et al. 2006, ApJ, 649, 382

Stella, L., Priedhorsky, W., & White, N. E. 1987, ApJL, 312, L17

Ströer, A., & Vecchio, A. 2006, CQGra, 23, 809

Strohmayer, T. E. 2005, ApJ, 627, 920

Szekerczes, K., Noble, S., Chirenti, C., & Thorpe, J. I. 2023, AJ, 166, 17

Tauris, T. M. 2018, PhRvL, 121, 131105

Tonry, J. L., Denneau, L., Heinze, A. N., et al. 2018, PASP, 130, 064505

van Paradijs, J., & McClintock, J. E. 1994, A&A, 290, 133

van Roestel, J., Kupfer, T., Green, M. J., et al. 2022, MNRAS, 512, 5440

Wevers, T., Torres, M. A. P., Jonker, P. G., et al. 2016, MNRAS, 462, L106

Wilhelm, M. J. C., Korol, V., Rossi, E. M., & D'Onghia, E. 2021, MNRAS, 500, 4958

Wood, M. A., Casey, M. J., Garnavich, P. M., & Haag, B. 2002, MNRAS, 334, 87

Zhao, G., Zhao, Y., Chu, Y., Jing, Y., & Deng, L. 2012, arXiv:1206.3569